

A Fast Adsorption of Azithromycin on Waste-Product-Derived Graphene Oxide Induced by H-Bonding and Electrostatic Interactions

Bushra Parvin Upoma, Sabina Yasmin,* Md. Aftab Ali Shaikh, Tajnin Jahan, Md. Anamul Haque, Mohammad Moniruzzaman, and Md Humayun Kabir*



Cite This: *ACS Omega* 2022, 7, 29655–29665



Read Online

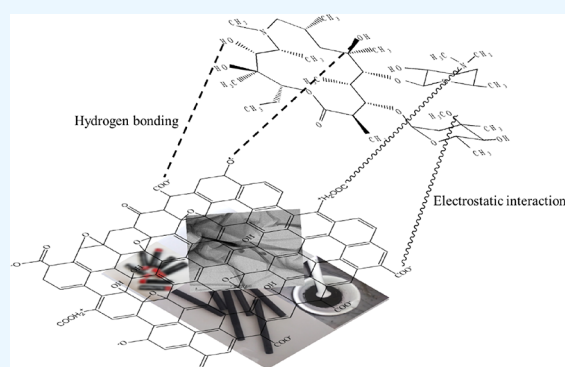
ACCESS |

Metrics & More

Article Recommendations

Supporting Information

ABSTRACT: Graphene oxide (GO) was prepared from the graphite electrode of waste dry cells, and the application of the prepared GO as a potential adsorbent for rapid and effective removal of an antibiotic, azithromycin (AZM), has been investigated. The synthesis process of GO is very simple, cost-effective, and eco-friendly. As-prepared GO is characterized by field-emission scanning electron microscopy, energy-dispersive X-ray, transmission electron microscopy, X-ray diffractometry, Fourier transform infrared spectroscopy, elemental analysis, Brunauer–Emmett–Teller sorptometry, and zeta potential analysis. The obtained GO has been employed for removal of the widely used AZM antibiotic from an aqueous solution. The quantitative analysis of AZM before and after adsorption has been carried out by liquid chromatography tandem mass spectrometry. The adsorption of AZM by GO was performed in a batch of experiments where the effects of adsorbent (GO) dose, solution pH, temperature, and contact time were investigated. Under optimum conditions (pH = 7.0, contact time = 15 min, and adsorbent dose = 0.25 g/L), 98.8% AZM was removed from the aqueous solution. The rapid and effective removal of AZM was significantly controlled by the electrostatic attractions and hydrogen bonding on the surface of GO. Adsorption isotherms of AZM onto GO were fitted well with the Freundlich isotherm model, while the kinetic data were fitted perfectly with the pseudo-second order. Therefore, the simple, cost-effective, and eco-friendly synthesis of GO from waste material could be applicable to fabricate an effective and promising low-cost adsorbent for removal of AZM from aqueous media.



1. INTRODUCTION

In recent years, antibiotics such as azithromycin (AZM), penicillin, trimethoprim, erythromycin, sulfamethoxazole, and metronidazole are the mostly used drugs for treating various diseases in humans, animals, modern husbandry, and aquaculture.¹ Excessive use of antibiotics can result in pollution of drinking water, surface/ground water, and even the ecosystem and aquatic environment.² Even in low amounts, antibiotics have huge negative impacts on the environment like high toxicity of algae and bacteria and bacterial resistance, inhibiting biological processes in waste water treatment and decreasing the rate of degradation of organic compounds.^{3,4} Southeast Asia is regarded to have the highest risk of antibiotics among all the regions. Antimicrobials are widely available as over-the-counter drugs in many of these countries; Bangladesh is one of them.^{5,6} Thus, the removal of widespread antibiotics has become a crucial issue.

Because of the treatment of various infectious diseases like skin disorders, there is malfunctioning of the respiratory system, diarrhea, intestinal inflammation, and sexually transmitted problems.^{7,8} AZM, a semi-synthetic macrolide anti-

biotic,⁹ is one of the most frequently used antibiotics. It is the prototype of azalides,¹⁰ which are chemically very close to macrolides related to erythromycin. AZM is a derivative of erythromycin; generally, it differs from erythromycin in a methyl-substituted nitrogen atom inserted into the lactone ring. It may cause bacterial resistance and thus result in ecological destruction and threaten the food chain. Therefore, it is urgent to reduce azithromycin from water environments.

Several more effective methods have been introduced to remove antibiotics from water environments. These include photolytic degradation,^{11–13} ozonation,¹⁴ coagulation,¹⁵ oxidation, biodegradation,¹⁶ ion exchange,¹⁷ membrane processing,¹⁸ chlorination,¹⁹ and adsorption.^{20,21} Among them,

Received: March 29, 2022

Accepted: August 11, 2022

Published: August 22, 2022



adsorption is regarded as the most capable method due to its remarkable benefits like a high efficiency, low cost, reliability, and being free from highly toxic byproducts.²² There are different kinds of adsorbents, like clay and minerals,²³ humic acid,¹⁹ activated carbon,²⁴ carbon nanotubes,²⁵ and graphene oxide (GO).²⁶ Even though the adsorption method for removing antibiotics has advantages, the inefficiency of adsorbent materials and difficulties of regeneration make them expensive and time-consuming for adsorption. To resolve these problems, it is urgent to design a cost-effective, efficient, and regenerable adsorbent with proper functional groups which are favorable for targeted adsorption by different types of interactions.

In recent years, graphene and GO-based materials have gained huge interest as a potential adsorbent for the removal of different types of antibiotics from water and waste water.²⁷ GO is one of the classical derivatives of graphene, which is an extension of the carbon nanomaterial produced by oxidation of the graphite layer.^{28,29} It has attracted unique scientific approaches in the field of electronics,³⁰ photonics,³¹ sensors,^{32–34} energy storage,³⁵ and adsorption.³⁶

The high theoretical surface area, abundance of surface functional groups, and high mechanical strength and conductivity make it a favorable adsorbent for water treatment.^{36,37} Pure GO is costly; therefore, it can be derived from waste dry-cell batteries. These batteries are non-rechargeable and non-recyclable; therefore, they get disposed in huge amounts worldwide. Unfortunately, these disposed dry cells deteriorate with time and the chemicals inside the batteries leach to the environment. Nevertheless, these used batteries would be a great source of graphite which can be utilized to derive GO.

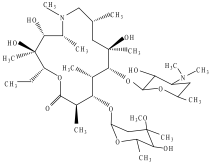
A number of reports are found on the study of AZM residues available in water. Faleye et al.³⁸ reported the availability of AZM residues in water bodies of Durban, South Africa, in the range of 1.3 ng/L. Rodriguez-Mozaz et al.³⁹ reported that the residue level of AZM in effluents of European wastewater treatment plants is 1500 ng/L. These contamination levels must appeal the attention of researchers to find a suitable removal technique of these pollutants from water.

In this study, GO has been synthesized from graphite electrodes of waste dry cells and it was employed as an adsorbent to remove AZM from an aqueous solution. To optimize the removal process, different batch experiments were carried out by varying the adsorbent dose, pH, temperature, and contact time. The obtained data were explained and correlated with different models of isotherms and kinetics studies.

2. EXPERIMENTAL SECTION

2.1. Chemicals. AZM (purity 99.5%) was collected from Radiant Pharmaceuticals Ltd. as a generous gift, and the chemical and physical characteristics of AZM are summarized in Table 1. LC–MS grade acetonitrile (ACN) and formic acid (FA) were purchased from AppliChem GmbH, Ottoweg, D-64291 Darmstadt, Germany. Potassium permanganate (KMnO₄) (≥99.0%, CAS: 7722-64-7) and sulfuric acid (H₂SO₄) (95–97%, reagent grade, CAS: 7664-93-9) were purchased from Scharlau, Spain. Phosphoric acid (H₃PO₄) (85 wt % in H₂O, CAS: 7664-38-2) was purchased from JANSSEN CHEMICA, Belgium. Ethanol (C₂H₅OH) (98%, CAS: 64-17-5) and hydrochloric acid (HCl) (37%, extra pure, CAS: 7647-

Table 1. Physical and Chemical Characteristics of AZM

Molecular formula	C ₃₈ H ₇₂ N ₂ O ₁₂
Molecular weight (g mol ⁻¹)	749.0
Water solubility (mg mL ⁻¹)	0.514
Melting point (°C)	113–115°C
Molecular structure	

01-0) were purchased from AppliChem, Germany. 30% hydrogen peroxide (H₂O₂) (30%, CAS: 7722-84-1) was purchased from Sigma-Aldrich. Ultrapure deionized (DI) water (18 MΩ cm) was used in the preparation of all the aqueous solutions.

2.2. Instrumentation. An Agilent LC module (1290 Infinity II) coupled with a triple quadrupole mass spectrometer (6420LC/TQ) was used for sample analysis. A ZORBAX RRHD Eclipse Plus C18 (2.1 × 100 mm, 1.8 μm particle size) was used for analytic separation. The binary mobile phase consists of 0.1% FA in water (A) and ACN (B). A linear isocratic mobile phase of 50% A and 50% B was used with a total flow of 0.3 mL/min. The analyte was analyzed in the liquid chromatography tandem mass spectrometry positive electron spray ionization mode (ESI⁺). Multiple reaction monitoring was performed with mass transition from 749.5 *m/z* to 591 *m/z* and 158 *m/z* as quantifier and qualifier ions, respectively. The dwell voltage was 110 V and the collision energy was 26 eV for both products ions. FTIR spectra were taken using a SHIMADZU IRAffinity-1 (Japan) spectrometer. The surface morphology and elemental composition of GO were observed by transmission electron microscopy (TEM) (model: Talos F200X, Thermo Fisher Scientific, accelerated voltage: 200 kV) and field emission scanning electron microscopy (FE-SEM) and energy-dispersive X-ray (EDX) (FE-SEM–EDX, JEOL-JSM-7610F, 0.1–30 kV, Netherlands). Elemental analysis was performed using a vario MICRO cube (Germany) elemental analyzer. The XRD patterns were measured using an X-ray diffractometer (model: SmartLab SE, Rigaku, Japan) with a Cu Kα source (λ = 1.541 Å). Nitrogen adsorption–desorption isotherms were characterized at –196 °C (77 K) using a PMI BET sorptometer (BET-201-A). The surface charge of GO was measured using a zeta potential analyzer (model: HORIBA scientific, SZ-100V2, Japan) in the pH range of 2–11.

2.3. Graphite Collection. Waste dry cells are used as a source of graphite powder. These waste dry cells were collected from households and market places. The dry cells were deconstructed carefully without disturbing the graphite rods held inside the cell. The graphite rods were then taken apart by using pliers, rubbed with paper, and cleaned with DI water to remove adhering paste MnO₂, NH₄Cl, and carbon. The fresh graphite rod was then air-dried and ground into fine powder with a mortar pestle. After that, the graphite powder was treated with Aqua Regia to remove inorganic impurities

Scheme 1. Schematic Illustration of the Preparation of Graphite Powder from Waste Dry Cells

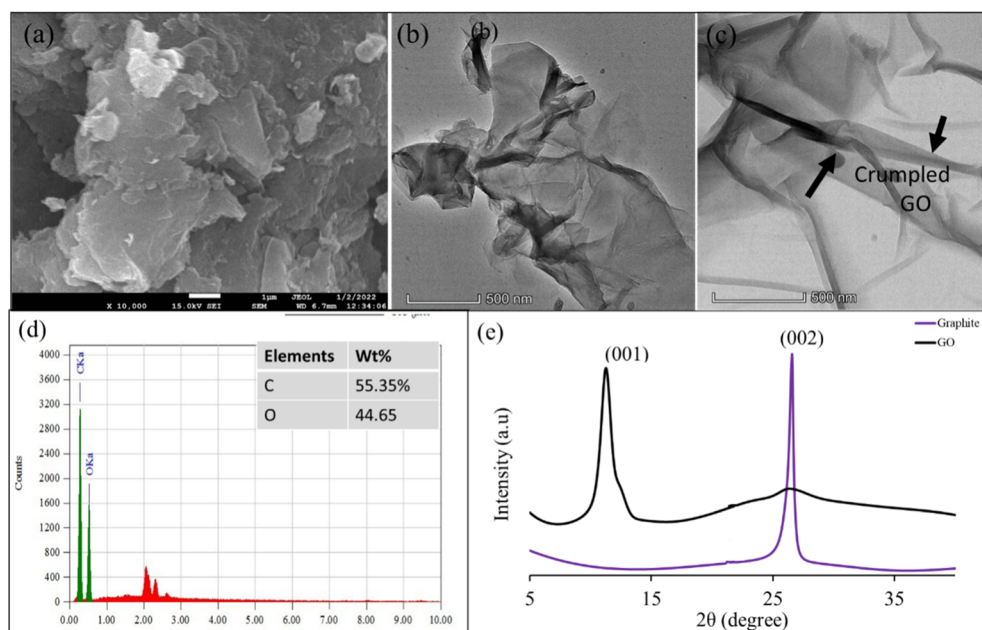
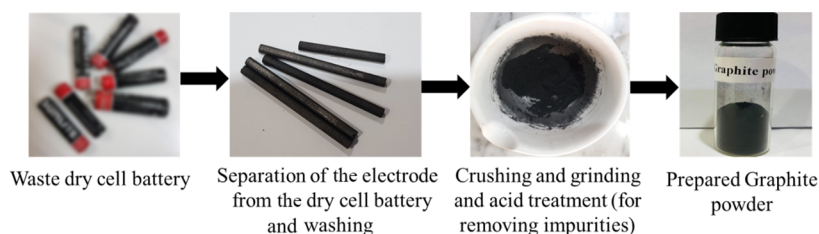


Figure 1. (a) FE-SEM image of GO, (b,c) TEM image of GO, (d) EDX plots of GO, and (e) XRD pattern of graphite and the GO adsorbent.

and was washed several times with DI water. Then it was dried at 60 °C for 24 h. Scheme 1 shows the schematic illustration of the preparation of graphite powder from waste dry cells.

2.4. Synthesis of GO. The synthesis of GO was accomplished by following a published modified procedure. GO was prepared by modified Hummers' method in two steps.^{40–42} Briefly, graphite powder (1 g) and KMnO_4 (6 g) were added slowly in a solution of H_2SO_4 (120 mL) and H_3PO_4 (14 mL) with continuous stirring. The mixture was heated for 6 h at 50 °C temperature and then cooled to room temperature and kept in an ice bath for 8 h to reduce the temperature, followed by slow addition of DI water (400 mL) and 30% H_2O_2 (3 mL) with constant stirring at nearly 4 °C. Then the reaction was stopped, and the mixture was centrifuged at 3500 rpm. The resultant product was then washed with water and 30% HCl. After that, it was again washed with water and finally with ethanol. Then as-prepared GO was dried under vacuum conditions to afford the GO powder.

2.5. Adsorption Study. AZM aqueous solutions were prepared with known concentrations. Specific amounts of the adsorbent GO were added to them, and then the samples were shaken for a targeted time at 250 rpm with a fixed temperature. After the contact time, samples were centrifuged at 3500 rpm to separate the adsorbent. To determine the optimum conditions for adsorption, the experiments were performed by changing the pH (2–11), adsorbent doses (2–10 mg), and contact time (5–120 min). Adjustment of pH was done by

adding 0.1 M HCl or 0.1 M NaOH to the solutions until a suitable pH is attained. Kinetic and thermodynamic studies were also conducted. For kinetics studies, the contact time was variable and the initial concentration was variable in isotherm studies. Thermodynamic studies were conducted at two different temperatures (30 and 40 °C).

The removal percentage was calculated by eq 1⁴³

$$\text{Removal percentage} = \frac{C_o - C_t}{C_o} \times 100 \quad (1)$$

The adsorbed amount at time t (q_t) and the amount adsorbed at equilibrium (q_e) were calculated by eqs 2 and 3

$$q_t = \frac{C_o - C_t}{M} \times V \quad (2)$$

$$q_e = \frac{C_o - C_e}{M} \times V \quad (3)$$

where C_o , C_t , and C_e are the initial concentration, the concentration at time t , and the equilibrium concentration of the AZM solution, respectively, (mg L^{-1}). M is the adsorbent dose in gram. V represents the volume of the AZM solution taken for batch experiments in liter (L).

3. RESULTS AND DISCUSSION

3.1. Characterization of the Adsorbent. **3.1.1. FE-SEM–EDX and TEM Analysis.** FE-SEM and TEM were employed to investigate the morphologies of synthesized GO. A soft flaky

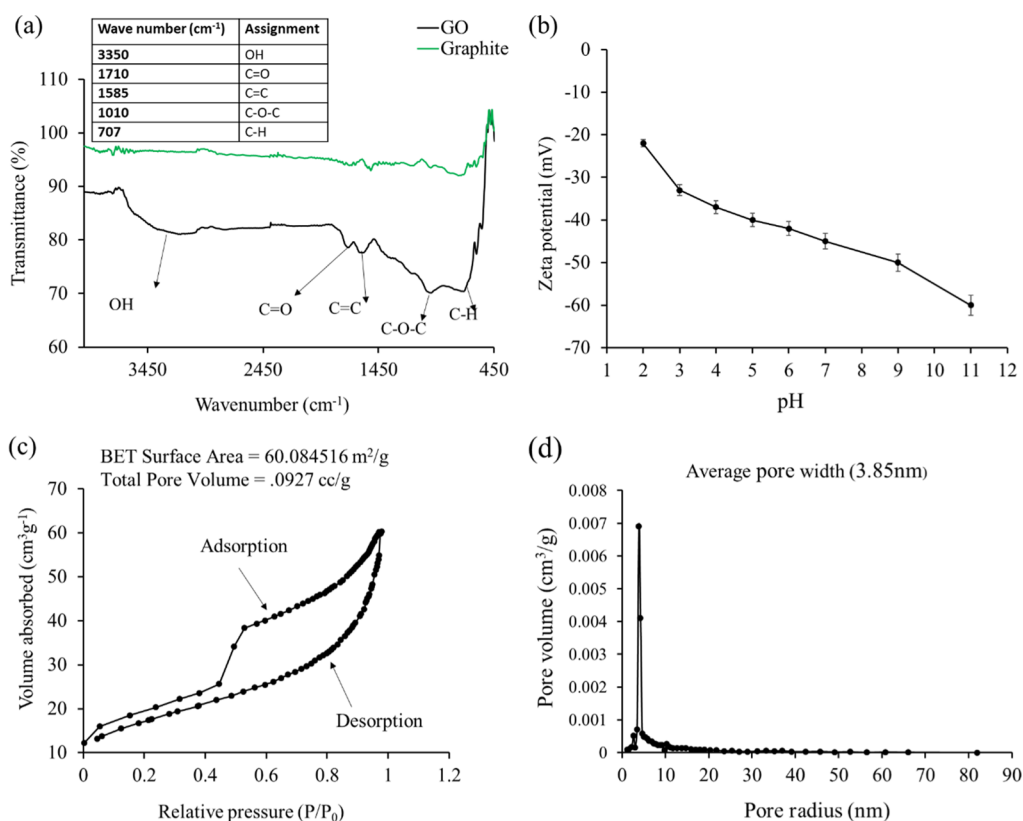


Figure 2. (a) FT-IR spectra of graphite and GO, (b) zeta potential of GO as a function of pH, and (c,d) Brunauer–Emmett–Teller N₂ adsorption/desorption isotherm and pore size distribution of GO.

texture reflecting its layered structure with irregular surface roughness and sheets of GO that are not well connected was observed, as shown in Figure 1a. Distorted graphene sheets were noticed due to the oxidation process of graphite to form GO; they also indicate the attachment of oxygen and other functional group with graphene to form GO.⁴⁴ These oxygenated functional groups in GO highly enhanced the attachment of targeted pollutants. Moreover, this surface roughness accounted for the large specific surface area, which would enhance the adsorption capability of GO.

The TEM image of GO (Figure 1b,c) shows shapes of thin stacked flakes having well-defined multilayered structures with many wrinkles. The multilayered wrinkled surface of GO formed due to scrolling and crumpling, which is an indication of the large surface of GO.⁴⁵

The EDX spectrum of GO as shown in Figure 1d indicated the presence of carbon (55.35%) and oxygen (44.65%) contents, which confirm the successful formation of GO.

3.1.2. XRD Analysis. The XRD patterns of graphite powder recovered from waste dry cells and GO are shown in Figure 1e. The diffraction peak of graphite is observed at $2\theta = 26.5^\circ$, corresponding to the (002) plane with an interlayer distance of 0.34 nm, which is in good agreement with the previous reports.^{46–48} After oxidation of graphite, the diffraction peak of GO appears at $2\theta = 11.4^\circ$ corresponding to the (001) plane with an interlayer spacing of 0.77 nm of the GO sheets, which was significantly greater than that of graphite powder (0.34 nm). This result indicated that many oxygenated functional groups were successfully incorporated to the regular graphite structure during the oxidation process and pushed the layers away and increased the interlayer distance.³⁰

3.1.3. FT-IR Analysis. Fourier transform infrared (FT-IR) spectra of graphite and GO are shown in Figure 2a. From the figure, it is observed that there is no significant peak for graphite. In contrast, the spectrum of GO shows several significant peaks because of the presence of oxygenated functional groups. The peaks appearing at 3350^{49,50} and 1710 cm⁻¹ originate from the stretching vibration of –OH (hydroxyl functional) and ketonic (C=O) groups.⁵¹ The two sharp peaks that appeared at 1010 and 1585 cm⁻¹ are characteristics of C–O–C stretching (epoxy groups) and aromatic C=C stretching, respectively.⁵² The peak observed at 707 cm⁻¹ is characteristic of the C–H bond from aromatic benzene.⁵³

Therefore, the results of the FT-IR spectra proved that GO was successfully prepared from graphite rods of waste dry cells and prepared GO is enriched with oxygen-containing functional groups which serve as active sites for the adsorption of AZM antibiotic.

3.1.4. Zeta Potential Analysis. The zeta potential (ζ) of GO was measured as a function of pH and is shown in Figure 2b. Negative ζ increases with the increase of pH and reached its highest value ($\zeta = -58.6$ mV) at pH 11. It reveals that the surface charge of the graphene sheet is negative. Therefore, it is concluded that oxygenated functional groups are located at the interface of GO sheets.⁵⁴

3.1.5. Brunauer–Emmett–Teller Analysis. A Brunauer–Emmett–Teller (BET) sorptometer was employed to determine the active surface area and porosity of the prepared adsorbent. The N₂ adsorption–desorption isotherm as well as pore size distribution of GO are shown in Figure 2c,d. The active specific surface area of GO is 60.0845 m²/g, as shown in Figure 2c. The pore size distribution was plotted according to

the Barrett–Joyner–Halenda (BJH) method from the N₂ desorption curve, and the pore radius was 3.85 nm. The total pore volume of GO (0.0927 cm³/g) found from waste dry cells is in good agreement with the GO prepared from commercially available graphite powder.^{53,55} It can be concluded that the use of graphite rods of dry cells is also a potential candidate instead of commercially available graphite powder.

3.1.6. Raman Analysis. Raman spectroscopy is commonly used to determine the crystal structure, defects, and disorder in graphene-based materials. The Raman spectrum of GO exhibits two prominent peaks (Figure S1) at around 1358 and 1594 cm⁻¹, corresponding to the D- and G-bands, respectively.⁵⁶ The D-band represents the defects or disorder of the GO system, while the G-band indicates the first-order stretching of sp²-bonded carbon atoms.^{30,56} The intensity ratio of the D- and G-bands (I_D/I_G) helps to measure the degree of disorder or functionalization.^{30,53} The calculated I_D/I_G ratio of GO is 0.88, and this result has similarities with the previous reported values.^{57,58} Moreover, the ratio of intensities of the D- and G-bands is also used to determine the number of layers. The I_D/I_G for GO was ~ 1 , indicating that prepared GO has a multilayer structure.⁵⁸

3.1.7. Elemental Analysis. The elemental composition of graphite powder and the prepared GO samples was analyzed by using an elemental (CHNS) analyzer (Table 2). The

Table 2. Results of Elemental Analysis of Graphite Powder and GO

material	C (%)	O (%)	H (%)	S (%)	N (%)	C/O
graphite	87.42		0.722	0.901		
GO	49.27	47.35	2.784	0.596		1.04

percentage of carbon was 87.42% in graphite rods, which reduced to 47.42% in the prepared GO. This suggests that many oxygen atoms were embedded into the carbon skeleton of graphite to form GO, which is consistent with the previous studies.^{58,59} In addition, H (2.784%) was present in GO, indicating enrichment of the oxygen-containing functional group. Meanwhile, the O content in GO was about 49.27% and the C to O ratio in prepared GO was almost around 1, from which we can conclude that our GO preparation is successfully done.⁵⁹

3.2. Adsorption of AZM on GO. The prepared GO was employed for removal of AZM from the aqueous solution of a concentration of 0.10 mg/L. The effects of pH, contact time, and adsorbent dose were analyzed, and the results are obtained.

3.2.1. pH. The removal of AZM from the aqueous solution was investigated at various pH to understand the effects of AZM ionization, adsorbent surface charge, and binding site efficiency.⁶⁰ From Figure 3a, it is observed that the removal efficiency of AZM remains nearly unchanged (97–98.8) % over the wide pH range of 2–11. The most interesting and excellent result over the long pH range can be explained based on the basis of the molecular structure and properties of both GO and AZM. The surface charge of GO becomes more negative with the increase of pH.

On the other hand, AZM may exist as cations when pH < 3.5, as zwitterions in the pH range of 3.5–7.7, and as anions at pH > 7.7.^{61,62} Generally, the adsorption of the adsorbate on the adsorbent occurs due to the mechanisms of hydrogen

bonding formation, electrostatic interactions, electron donor–acceptor interactions, and pi–pi interactions.⁶³ In this study, 98.60% adsorption occurs at low pH (~ 2) due to the domain hydrogen bonding over the electrostatic attraction.⁶⁴ Although removal of AZM remains nearly unchanged over the wide pH range, slightly low adsorption (97.5% adsorption) at pH 5 and slightly higher adsorption ($\approx 98.8\%$ adsorption) in the pH range of 7–11 were noticed. A slight increase (97.5 to 98.8%) in the adsorption of AZM can be explained in terms of adsorbent deprotonation and the formation of negatively charged that ultimately favor the electrostatic attraction between negatively charged GO and the positively charged carbon of the –O–CH₃ group present.

We observed slightly low adsorption at pH 5 (97.5% adsorption). After increasing the pH from 7–11, the adsorption slightly increases ($\approx 98.8\%$ adsorption). A slight increase in the adsorption of AZM pH (7–11) can be explained in terms of adsorbent deprotonation and the negative charge, which favor the electrostatic attraction between the negatively charged adsorbent and the –CH₃ group of AZM.³ Since pH has a negligible effect in the range of 2–11 for the adsorptive removal of AZM from water, optimum conditions at pH 7 were chosen for further experiments.

3.2.2. Contact Time. The influence of contact time on the adsorption process is one of the most important factors for the enhanced removal of target pollutants.²¹ To investigate the influence of contact time on the removal of AZM, the experiments were performed in the range of 5–120 min. The removal percentages of AZM are shown as a function of contact time (Figure 3b). Most of the AZM (87%) was removed in 5 min. The removal percentages were increased with the increase of contact time. The maximum adsorption (98.8%) occurred at 15 min and remained nearly constant with a further increase of contact time (up to 120 min). Therefore, the equilibrium time for optimum adsorption of AZM is considered as 15 min. The very fast removal of AZM using this GO adsorbent is rarely found. The excellent removal efficiency is attributed to the versatile property of GO as the adsorbent through the electrostatic interaction and hydrogen bond formation.

3.2.3. Adsorbent Dose. AZM was adsorbed by various amounts of GO from 2 to 12 mg for investigating the effect of adsorbent dose on the removal efficiency (Figure 3c). The concentration of AZM was kept constant (0.10 mg/L) for this experiment. At a low adsorbent dose (2 mg), the removal efficiency was 97.7% and increased with increasing dose. The maximum adsorption efficiency (98.8%) was found for the dose of 5 mg. Above this dose, the efficiency decreased and remained constant up to 12 mg. The increase of removal efficiency (97.7 to 98.8%) with increasing dose from 2 to 5 mg is in good agreement with the previous study where zeolite was used as an adsorbent.⁶⁵ The decrease of removal efficiency (98.8 to 95.5%) is due to the fact that the aggregation of the adsorbent by their intermolecular attraction occurred at an elevated dose. It can be noted that the optimum dose of GO is 5 mg (0.25 g/L).

3.3. Adsorption Mechanism. Generally, the adsorption mechanism of different organic compounds on GO is explained on the basis of H-bonding,⁶⁶ electrostatic interactions,^{67,68} and π – π interactions.^{69,70} GO used in this study are enriched with π -electrons and different oxygenated functional groups that can play an important role for the

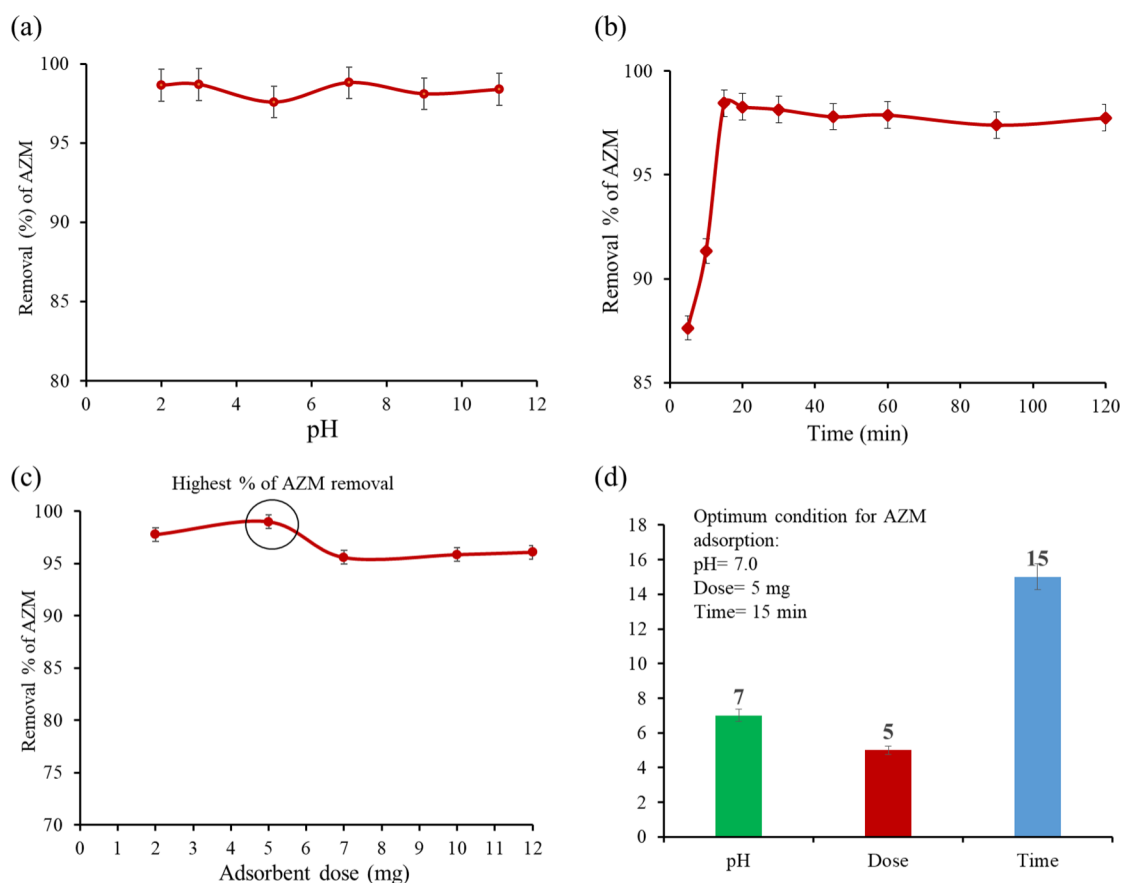


Figure 3. (a) Effect of pH on the adsorption of AZM from the aqueous solution by GO ($C_o = 100$ ppb, GO = 0.25 g/L, $t = 15$ min, shaking = 200 rpm, $T = 25$ °C), (b) effect of contact time on the adsorption of AZM by GO ($C_o = 100$ ppb, GO = 0.25 g/L, pH = 7, shaking = 200 rpm, $T = 25$ °C), (c) effect of adsorbent dose on the adsorption of AZM from the aqueous solution onto GO ($C_o = 100$ ppb, pH = 7, $t = 15$ min, shaking = 200 rpm, $T = 25$ °C), and (d) summary of optimum conditions.

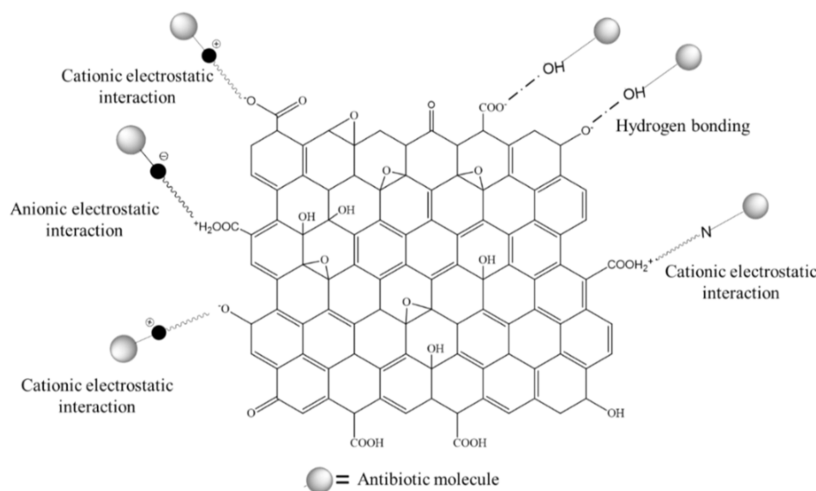


Figure 4. Various adsorption interaction mechanisms of antibiotics on the GO adsorbent.

adsorption mechanism between GO and AZM through H-bonds, electrostatic interactions, and π - π interactions.⁷¹ AZM is enriched with $-\text{OH}$, $-\text{CH}_3$, $=\text{O}$, $-\text{O}-$, $-\text{N}-$, $-\text{N}=\text{}$, and $-\text{OCH}_3$ functional groups in which $-\text{OH}$ involves to form H-bonds, and $=\text{O}$, $-\text{O}-$, $-\text{N}-$, $-\text{N}=\text{}$, and $-\text{O}-\text{CH}_3$ groups involve in anionic electrostatic interactions, while the $-\text{CH}_3$ group participates in cationic electrostatic interactions. The possible adsorption interactions between AZM and GO are

shown in Figure 4. Since there is no π -electron in AZM, it is unlikely to have π - π interactions with GO. In the present study, fast adsorption occurs presumably due to the formation of cationic and anionic electrostatic interactions and H-bonding between AZM and GO.

3.4. Kinetic Model of Adsorption. The study of adsorption kinetics deals with the nature and interaction (physical and/or chemical) of adsorbent and adsorbate

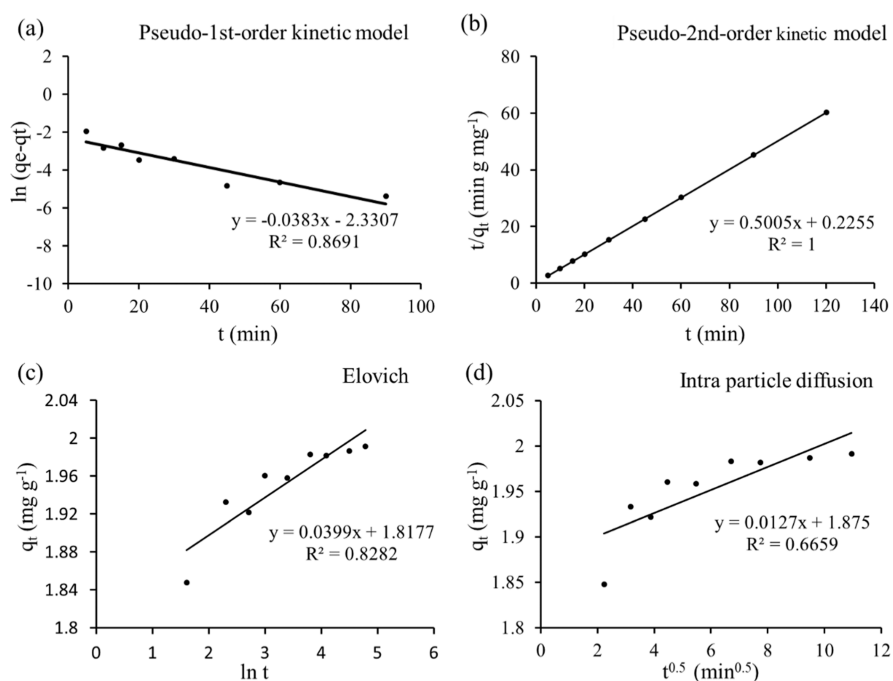


Figure 5. (a) Pseudo-first-order kinetic model, (b) pseudo-second-order kinetic model, (c) Elovich kinetic model, and (d) Weber–Morris intraparticle diffusion model [conditions: $C_0 = 500$ ppb, $\text{pH} = 7$, $\text{GO} = 0.25$ g/L, $t = (5\text{--}120)$ mins, shaking = 200 rpm, $T = 25$ °C].

Table 3. Parameters Calculated from the Kinetic Models

kinetic model	curve fitting	parameters	0.5 mg/L AZM	
pseudo-first order	linear	q_e	(mg g ⁻¹)	0.0972
		k_1	(g mg ⁻¹ min ⁻¹)	-0.0383
		R^2		0.8691
pseudo-second order	linear	q_e	(mg g ⁻¹)	2.0
		k_2	(g mg ⁻¹ min ⁻¹)	1.111
		R^2		1.0000
Elovich	linear	a_e	(mg g ⁻¹ min ⁻¹)	2.41×10^{18}
		b_e	(g mg ⁻¹)	25.06
		R^2		0.8282
intraparticle diffusion	linear	k_i	(mg g ⁻¹ min ^{-0.5})	0.0127
		R^2		0.6659
		C_i	(mg g ⁻¹)	1.875

species.⁷¹ For kinetic models, 5 mg of GO was added to 20 mL of AZM (concentration 0.5 mg/L) and the absorption of AZM on GO was performed at various time intervals from 5 to 120 min while the mixture solution was kept at 200 rpm. For the investigation of the kinetics data, Lagergren's pseudo-first-order, Ho's pseudo-second-order, Elovich, and Weber–Morris intraparticle diffusion models were considered. The linearized forms of the pseudo-first-order, pseudo-second-order, Elovich, and Weber–Morris intraparticle diffusion models are expressed by eqs 4–7, respectively,⁴³

$$\ln(q_e - q_t) = \ln q_e - k_1 t \quad (4)$$

$$\frac{t}{q_t} = \frac{1}{k_2 q_e^2} + \frac{t}{q_e} \quad (5)$$

$$q_t = \frac{\ln a_e b_e}{b_e} + \frac{1}{b_e} \ln t \quad (6)$$

$$q_t = k_i t^{0.5} + C_i \quad (7)$$

where q_e is the adsorbed amount at equilibrium, mg g⁻¹; q_t is the adsorbed amount at time t , mg g⁻¹; k_1 is the rate constant associated with the pseudo-first-order model, g mg⁻¹ min⁻¹; k_2 is the rate constant associated with the pseudo-second-order model, g mg⁻¹ min⁻¹; a_e is regarded as the initial adsorption rate, mg g⁻¹ min⁻¹; b_e is related to the magnitude of surface coverage and activation energy for chemisorption, g mg⁻¹; k_i is the rate constant associated with the intraparticle diffusion model, mg g⁻¹ min^{-0.5}; and C_i is a constant and proportional to boundary layer thickness, mg g⁻¹.

In various kinetic models, the experimental data were fitted with the linearized form of the model equation as shown in Figure 5a–d. Different kinetic parameters of AZM adsorption on GO are summarized in Table 3. The correlation coefficients (R^2) for pseudo-first-order, pseudo-second-order, Elovich, and intraparticle diffusion are 0.8690, 1.0000, 0.8282, and 0.6659, respectively. Considering R^2 values, the kinetic data are well fitted with the pseudo-second-order model, which indicates that the rate-determining step may be chemisorption involving valence forces through sharing or exchange of electrons between the adsorbent and adsorbate.⁷²

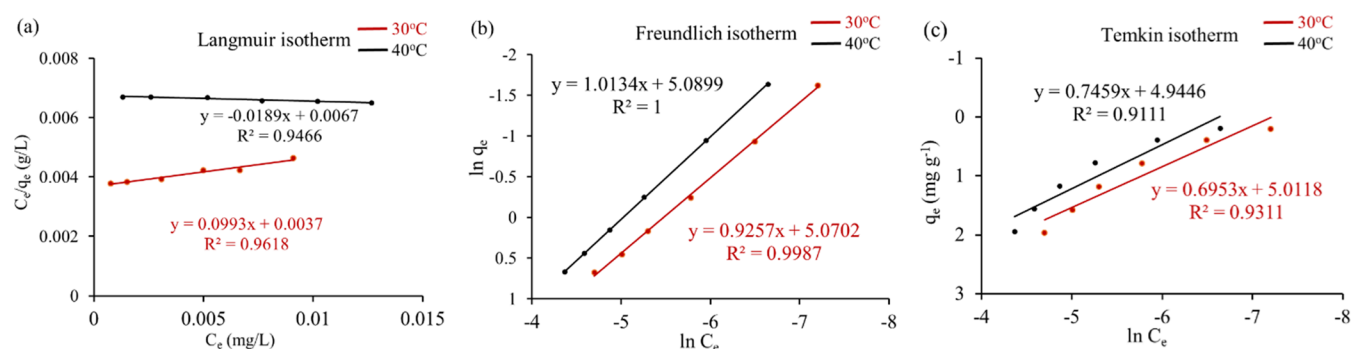


Figure 6. (a) Langmuir isotherms, (b) Freundlich isotherms, and (c) Temkin isotherm model (conditions: $C_0 = 50\text{--}500$ ppb, pH = 7, GO = 0.25 g/L, $t = 15$ min, shaking = 200 rpm, $T = 30$ and 40 °C).

Table 4. Parameters Calculated from Isotherm Models

isotherm model	curve fitting	parameters	30 °C	40 °C
Langmuir	linear	q_m (mg g^{-1})	16.18	55.55
		K_L (L mg^{-1})	26.83	2.82
		R^2	0.9618	0.9466
Freundlich	linear	K_F ($\text{mg}^{1-1/n}\text{L}^{-1/n} \text{g}^{-1}$)	150.17	140.41
		n	1.01	1.0
		R^2	0.9987	1.0
Temkin	linear	K_T (L g^{-1})	1350.33	874.01
		b (J mol^{-1})	3623.31	3377.52
		R^2	0.9311	0.9111

3.5. Adsorption Isotherm. The adsorption isotherms describe the interaction between the adsorbate and adsorbent at constant temperature and pH. The adsorption isotherm was investigated by varying the AZM concentration from 0.05 to 0.5 mg/L. The batch adsorption process was conducted using 5 mg (20 mL) of GO at pH 7 for 15 min while shaking at 30 and 40 °C, Figure 6a–c. For adsorption isotherms, experimental data were fitted to Langmuir, Freundlich, and Temkin, models.⁵³ The linear forms of the Langmuir, Freundlich, and Temkin isotherm models are expressed by eqs 8–9^{10,53,73}

$$\frac{C_e}{q_e} = \frac{C_e}{q_m} + \frac{1}{K_L q_m} \quad (8)$$

$$\ln q_e = \ln K_F + \frac{1}{n} \ln C_e \quad (9)$$

$$q_e = \frac{RT}{b} \ln K_T + \frac{RT}{b} \ln C_e \quad (10)$$

where C_e is the concentration of AZM at equilibrium, mg L^{-1} ; q_e is the adsorbed amount at equilibrium, mg g^{-1} ; q_m is the maximum adsorption capacity of GO at monolayer coverage, mg g^{-1} ; K_L refers to the dimensionless Langmuir adsorption constant; K_F refers to the Freundlich adsorption constant, $\text{mg}^{1-1/n}\text{L}^{-1/n} \text{g}^{-1}$; n is a constant related to adsorption intensity; R is the universal gas constant, $\text{J K}^{-1} \text{mol}^{-1}$; T is the temperature, K; K_T denotes the equilibrium binding constant, L g^{-1} ; and b is a constant related to the heat of adsorption, J mol^{-1} .

The data were fitted with these models as shown in Figure 6a–c, and the fitting parameters for AZM are listed in Table 4. From the R^2 values of all models, it is apparent that Freundlich isotherms ($R^2 = 0.998$) are in good agreement in comparison to the Langmuir ($R^2 = 0.9618$) and Temkin isotherms ($R^2 =$

0.9318) at both 30 and 40 °C. The Freundlich adsorption isotherms describe that the adsorption of AZM by GO is a multilayer adsorption process on heterogeneous surfaces. On the other hand, reasonable fitting of the Temkin model reveals the electrostatic interaction in the adsorption process.

3.6. Comparison of the GO Adsorbent with Other Adsorbents. The maximum adsorption capacities of GO have been compared with those of the other adsorbents reported in the previous literature (Table 5). It is observed that GO showed higher adsorption capacity compared to the other adsorbents, even though some of these adsorbents required a more complicated preparation method. Time is another important factor in adsorption study. In this study, the adsorption equilibrium was found in just 15 min, which is the fastest among the reports found (Table 5).

Table 5. Comparison of AZM Adsorption Capacity and Equilibrium Time with Those of the Previous Literature^a

antibiotic	adsorbent	adsorption capacity (mg/g)	time	reference
AZM	NC	28.011	7 h	62
	NC-Tween	37.635	7 h	62
	NC-Triton	44.64	7 h	62
	PAC/Fe/Si/Zn nanocomposite	7.93	120 min	74
	FAU-2 zeolite	8.85	30 min	75
	activated carbon (AC)	41.84	120 min	43
	magnetic activated carbon (MAC)	42.37		43
	GO@Fe ₃ O ₄ /ZnO/SnO ₂	9.375	30 min	76
	GO (derived from waste dry cells)	55.55	15 min	this study

^aNC—natural clinoptilolite, FAU—Faujasite-type zeolites, PAC—activated carbon powder.

3.7. Stability and Reusability. The stability and reusability of an adsorbent are very important issues for environmental and economic reasons. After adsorption of AZM, GO was successfully regenerated by the treatment with acetone. GO can be reused and recycled nine times, as shown in Figure 7. The removal percentage of GO was slightly

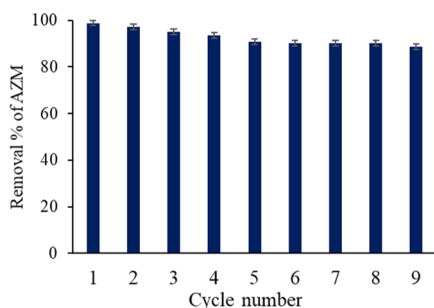


Figure 7. Stability and reusability test for the GO adsorbent.

decreased from 98.8 to ~90% after nine successive cycles and gained stability in further washing. On the basis of this study, GO could be used for the multiple adsorptions in which the regeneration of adsorbents would reduce the operation costs.

4. CONCLUSIONS

In the present study, GO as a potential adsorbent has been prepared from graphite rods of waste dry cells, and the adsorption of the AZM antibiotic on the adsorbent was investigated. Prepared GO was characterized using FE-SEM, EDX, TEM, XRD, FT-IR, elemental analysis, BET sorptometry, and zeta potential analysis. Various oxygen-containing functional groups of GO enhance the removal process of AZM through cationic and anionic electrostatic interactions and H-bonding between them. The key parameters such as pH, contact time, and adsorbent dose were regulated to achieve the optimum conditions for adsorption. The adsorption of AZM on GO occurred rapidly, and the maximum adsorption (98.8%) was attained within a very short time (15 min) using a small adsorbent dose of 0.25 g/L. The adsorption kinetics follows the pseudo-second-order model, suggesting the interaction of AZM with GO through electrostatic interactions and H-bonding. The adsorption isotherms were well fitted with the Freundlich model and reasonably fitted with the Temkin model, indicating that the adsorption of AZM by GO is multilayer adsorption. Finally, GO was found to be an efficient, effective, regenerable, and reuseable adsorbent for the fast adsorption of the AZM antibiotic from aqueous media. Waste-dry-cell-derived GO could open a new pathway to find an alternative adsorbent for remediation of AZM from aqueous environments.

■ ASSOCIATED CONTENT

Supporting Information

The Supporting Information is available free of charge at <https://pubs.acs.org/doi/10.1021/acsomega.2c01919>.

Raman spectra and I_D/I_G ratio of GO (PDF)

■ AUTHOR INFORMATION

Corresponding Authors

Sabina Yasmin – Institute of National Analytical Research and Service (INARS), Bangladesh Council of Scientific and

Industrial Research (BCSIR), Dhaka 1205, Bangladesh;

Email: sabinayasmin@bcsir.gov.bd

Md Humayun Kabir – Institute of National Analytical Research and Service (INARS), Bangladesh Council of Scientific and Industrial Research (BCSIR), Dhaka 1205, Bangladesh; Central Analytical and Research Facilities (CARF), BCSIR, Dhaka 1205, Bangladesh; orcid.org/0000-0002-1411-0943; Email: humayunkabir@bcsir.gov.bd

Authors

Bushra Parvin Upoma – Institute of National Analytical Research and Service (INARS), Bangladesh Council of Scientific and Industrial Research (BCSIR), Dhaka 1205, Bangladesh

Md. Aftab Ali Shaikh – Institute of National Analytical Research and Service (INARS), Bangladesh Council of Scientific and Industrial Research (BCSIR), Dhaka 1205, Bangladesh; Department of Chemistry, University of Dhaka, Dhaka 1000, Bangladesh

Tajnin Jahan – Institute of National Analytical Research and Service (INARS), Bangladesh Council of Scientific and Industrial Research (BCSIR), Dhaka 1205, Bangladesh

Md. Anamul Haque – Department of Chemistry, University of Dhaka, Dhaka 1000, Bangladesh; orcid.org/0000-0002-2461-9532

Mohammad Moniruzzaman – Central Analytical and Research Facilities (CARF), BCSIR, Dhaka 1205, Bangladesh

Complete contact information is available at:

<https://pubs.acs.org/10.1021/acsomega.2c01919>

Notes

The authors declare no competing financial interest.

■ ACKNOWLEDGMENTS

The authors are grateful to the Bangladesh Council of Scientific and Industrial Research (BCSIR) for financial support (R&D ref. no. 39.02.0000.011.14.134.2021/900, date 30.12.2021) and facilities. The assistance from CARF, BTRI, and BAEC to perform BET analysis, XRD, FE-SEM, and TEM is appreciated. The authors are also thankful to the Ministry of Science and Technology for providing special allocation (ref no. 39.00.0000.009.14.019.21-ES-401/1148, date: 15/12/2021). Radiant Pharmaceuticals Ltd. Bangladesh is acknowledged for their assistance, standard, and reagent support.

■ REFERENCES

- (1) Kümmerer, K. Antibiotics in the Aquatic Environment—A Review—Part I. *Chemosphere* **2009**, *75*, 417–434.
- (2) Talaiekhazani, A.; Joudaki, S.; Banisharif, F.; Eskandari, Z.; Cho, J.; Moghadam, G.; Rezaia, S. Comparison of Azithromycin Removal from Water Using UV Radiation, Fe (VI) Oxidation Process and ZnO Nanoparticles. *Int. J. Environ. Res. Publ. Health* **2020**, *17*, 1758.
- (3) Davoodi, S.; Dahrzama, B.; Goudarzi, N.; Gorji, H. G. Adsorptive Removal of Azithromycin from Aqueous Solutions Using Raw and Saponin-Modified Nano Diatomite. *Water Sci. Technol.* **2019**, *80*, 939–949.
- (4) Watkinson, A. J.; Murby, E. J.; Kolpin, D. W.; Costanzo, S. D. The Occurrence of Antibiotics in an Urban Watershed: From Wastewater to Drinking Water. *Sci. Total Environ.* **2009**, *407*, 2711–2723.

- (5) Chereau, F.; Opatowski, L.; Tourdjman, M.; Vong, S. Risk Assessment for Antibiotic Resistance in South East Asia. *BMJ* **2017**, *358*, j3393.
- (6) Hossain, A.; Nakamichi, S.; Habibullah-Al-Mamun, M.; Tani, K.; Masunaga, S.; Matsuda, H. Occurrence and Ecological Risk of Pharmaceuticals in River Surface Water of Bangladesh. *Environ Res* **2018**, *165*, 258–266.
- (7) Chen, B.-M.; Liang, Y.-Z.; Chen, X.; Liu, S.-G.; Deng, F.-L.; Zhou, P. Quantitative Determination of Azithromycin in Human Plasma by Liquid Chromatography–Mass Spectrometry and Its Application in a Bioequivalence Study. *J. Pharmaceut. Biomed. Anal.* **2006**, *42*, 480–487.
- (8) Drew, R. H.; Gallis, H. A. Azithromycin—Spectrum of Activity, Pharmacokinetics, and Clinical Applications. *Pharmacotherapy* **1992**, *12*, 161–173.
- (9) Yang, Z. Y.; Wang, L.; Tang, X. Determination of Azithromycin by Ion-Pair HPLC with UV Detection. *J. Pharm. Biomed. Anal.* **2009**, *49*, 811–815.
- (10) Lalak, N. J.; Morris, D. L. Azithromycin Clinical Pharmacokinetics. *Clin. Pharmacokinet.* **1993**, *25*, 370–374.
- (11) Sharma, S. K.; Kumar, A.; Sharma, G.; Stadler, F. J.; Naushad, Mu.; Ghfar, A. A.; Ahamad, T. LaTiO₂N/Bi₂S₃ Z-Scheme Nano Heterostructures Modified by RGO with High Interfacial Contact for Rapid Photocatalytic Degradation of Tetracycline. *J. Mol. Liq.* **2020**, *311*, 113300.
- (12) Sharma, G.; Gupta, V. K.; Agarwal, S.; Bhogal, S.; Naushad, Mu.; Kumar, A.; Stadler, F. J. Fabrication and Characterization of Trimetallic Nano-Photocatalyst for Remediation of Ampicillin Antibiotic. *J. Mol. Liq.* **2018**, *260*, 342–350.
- (13) Akter, S.; Islam, Md. S.; Kabir, Md. H.; Shaikh, Md. A. A.; Gafur, Md. A. UV/TiO₂ Photodegradation of Metronidazole, Ciprofloxacin and Sulfamethoxazole in Aqueous Solution: An Optimization and Kinetic Study. *Arab. J. Chem.* **2022**, *15*, 103900.
- (14) Khan, M. H.; Bae, H.; Jung, J.-Y. Tetracycline Degradation by Ozonation in the Aqueous Phase: Proposed Degradation Intermediates and Pathway. *J. Hazard Mater.* **2010**, *181*, 659–665.
- (15) Li, N.; Sheng, G.-P.; Lu, Y.-Z.; Zeng, R. J.; Yu, H.-Q. Removal of Antibiotic Resistance Genes from Wastewater Treatment Plant Effluent by Coagulation. *Wat. Res.* **2017**, *111*, 204–212.
- (16) Crini, G.; Lichtfouse, E.; Wilson, L. D.; Morin-Crini, N. Conventional and Non-Conventional Adsorbents for Wastewater Treatment. *Environ. Chem. Lett.* **2019**, *17*, 195–213.
- (17) Wang, Y.-J.; Jia, D.-A.; Sun, R.-J.; Zhu, H.-W.; Zhou, D.-M. Adsorption and Cosorption of Tetracycline and Copper(II) on Montmorillonite as Affected by Solution PH. *Environ. Sci. Technol.* **2008**, *42*, 3254–3259.
- (18) Koyuncu, I.; Arikan, O. A.; Wiesner, M. R.; Rice, C. Removal of Hormones and Antibiotics by Nanofiltration Membranes. *J. Membr. Sci.* **2008**, *309*, 94–101.
- (19) Gu, C.; Karthikeyan, K. G.; Sibley, S. D.; Pedersen, J. A. Complexation of the Antibiotic Tetracycline with Humic Acid. *Chemosphere* **2007**, *66*, 1494–1501.
- (20) Miao, J.; Wang, F.; Chen, Y.; Zhu, Y.; Zhou, Y.; Zhang, S. The Adsorption Performance of Tetracyclines on Magnetic Graphene Oxide: A Novel Antibiotics Absorbent. *Appl. Surf. Sci.* **2019**, *475*, 549–558.
- (21) Esmaeili Bidhendi, M.; Poursorkh, Z.; Sereshti, H.; Rashidi Nodeh, H.; Rezaia, S.; Afzal Kamboh, M. Nano-Size Biomass Derived from Pomegranate Peel for Enhanced Removal of Cefixime Antibiotic from Aqueous Media: Kinetic, Equilibrium and Thermodynamic Study. *Int. J. Environ. Res. Publ. Health* **2020**, *17*, 4223.
- (22) Crini, G.; Lichtfouse, E. Advantages and Disadvantages of Techniques Used for Wastewater Treatment. *Environ. Chem. Lett.* **2019**, *17*, 145–155.
- (23) Guler, U. A.; Sarioglu, M. Removal of Tetracycline from Wastewater Using Pumice Stone: Equilibrium, Kinetic and Thermodynamic Studies. *J. Environ. Health Sci. Eng.* **2014**, *12*, 79.
- (24) Choi, K.-J.; Kim, S.-G.; Kim, S.-H. Removal of Antibiotics by Coagulation and Granular Activated Carbon Filtration. *J. Hazard Mater.* **2008**, *151*, 38–43.
- (25) Jiang, L.; Tu, H.; Lu, Y.; Wu, Y.; Tian, J.; Shi, X.; Wang, Q.; Zhan, Y.; Huang, Z.; Deng, H. Spherical and Rodlike Inorganic Nanoparticle Regulated the Orientation of Carbon Nanotubes in Polymer Nanofibers. *Chem. Phys. Lett.* **2016**, *650*, 82–87.
- (26) Ouyang, K.; Zhu, C.; Zhao, Y.; Wang, L.; Xie, S.; Wang, Q. Adsorption Mechanism of Magnetically Separable Fe₃O₄/Graphene Oxide Hybrids. *Appl. Surf. Sci.* **2015**, *355*, 562–569.
- (27) Zhang, X.; Gao, B.; Creamer, A. E.; Cao, C.; Li, Y. Adsorption of VOCs onto Engineered Carbon Materials: A Review. *J. Hazard Mater.* **2017**, *338*, 102–123.
- (28) Yasmin, S.; Cho, S.; Jeon, S. Electrochemically Reduced Graphene-Oxide Supported Bimetallic Nanoparticles Highly Efficient for Oxygen Reduction Reaction with Excellent Methanol Tolerance. *Appl. Surf. Sci.* **2018**, *434*, 908.
- (29) Yasmin, S.; Joo, Y.; Jeon, S. 2,3-Diaminopyridine Functionalized Reduced Graphene Oxide-Supported Palladium Nanoparticles with High Activity for Electrocatalytic Oxygen Reduction Reaction. *Appl. Surf. Sci.* **2017**, *406*, 226.
- (30) Roy, I.; Sarkar, G.; Mondal, S.; Rana, D.; Bhattacharyya, A.; Saha, N. R.; Adhikari, A.; Khastgir, D.; Chattopadhyay, S.; Chattopadhyay, D. Synthesis and Characterization of Graphene from Waste Dry Cell Battery for Electronic Applications. *RSC Adv.* **2016**, *6*, 10557–10564.
- (31) Wu, J.; Jia, L.; Zhang, Y.; Qu, Y.; Jia, B.; Moss, D. J. Graphene Oxide for Integrated Photonics and Flat Optics. *Adv. Mater.* **2021**, *33*, 2006415.
- (32) Yasmin, S.; Ahmed, D.; Park, S.; Jeon, S. Nitrogen-Doped Graphene Supported Cobalt Oxide for Sensitive Determination of Dopamine in Presence of High Level Ascorbic Acid. *J. Electrochem. Soc.* **2016**, *163*, B491–B498.
- (33) Yasmin, S.; Ahmed, M. S.; Jeon, S. Determination of Dopamine by Dual Doped Graphene-Fe₂O₃ in Presence of Ascorbic Acid. *J. Electrochem. Soc.* **2015**, *162*, B363.
- (34) Roy, N.; Yasmin, S.; Jeon, S. Effective Electrochemical Detection of Dopamine with Highly Active Molybdenum Oxide Nanoparticles Decorated on 2, 6 Diaminopyridine/Reduced Graphene Oxide. *Microchem. J.* **2020**, *153*, 104501.
- (35) Yasmin, S.; Mohammad, S.; Ahmed, S.; Jeon, S. Nitrogen-Doped Graphene Supported Cobalt Oxide Nanocomposite as High Performance Electrocatalyst for Oxygen Reduction Reaction. *J. Nanosci. Nanotechnol.* **2016**, *16*, 3959.
- (36) Zhu, H.; Chen, T.; Liu, J.; Li, D. Adsorption of Tetracycline Antibiotics from an Aqueous Solution onto Graphene Oxide/Calcium Alginate Composite Fibers. *RSC Adv.* **2018**, *8*, 2616–2621.
- (37) Li, D.; Liu, J.; Barrow, C. J.; Yang, W. Protein Electrochemistry Using Graphene-Based Nano-Assembly: An Ultrasensitive Electrochemical Detection of Protein Molecules via Nanoparticle–Electrode Collisions. *Chem. Commun.* **2014**, *50*, 8197–8200.
- (38) Faleye, A. C.; Adegoke, A. A.; Ramluckan, K.; Fick, J.; Bux, F.; Stenström, T. A. Concentration and Reduction of Antibiotic Residues in Selected Wastewater Treatment Plants and Receiving Waterbodies in Durban, South Africa. *Sci. Total Environ.* **2019**, *678*, 10–20.
- (39) Rodriguez-Mozaz, S.; Vaz-Moreira, I.; Varela Della Giustina, S.; Llorca, M.; Barceló, D.; Schubert, S.; Berendonk, T. U.; Michael-Kordatou, I.; Fatta-Kassinos, D.; Martinez, J. L.; Elpers, C.; Henriques, I.; Jaeger, T.; Schwartz, T.; Paulshus, E.; O’Sullivan, K.; Pärnänen, K. M. M.; Virta, M.; Do, T. T.; Walsh, F.; Manaia, C. M. Antibiotic Residues in Final Effluents of European Wastewater Treatment Plants and Their Impact on the Aquatic Environment. *Environ. Int.* **2020**, *140*, 105733.
- (40) Alkhouzaam, A.; Qiblawey, H.; Khraisheh, M.; Atieh, M.; Al-Ghouti, M. Synthesis of Graphene Oxides Particle of High Oxidation Degree Using a Modified Hummers Method. *Ceram. Int.* **2020**, *46*, 23997–24007.
- (41) Roy, N.; Yasmin, S.; Ejaz, A.; Soon Han, H.; Jeon, S. Influence of Pyrrolic and Pyridinic-N in the Size and Distribution Behaviour of

- Pd Nanoparticles and ORR Mechanism. *Appl. Surf. Sci.* **2020**, *533*, 147500.
- (42) Upoma, B. P.; Mahnaz, F.; Rahman Sajal, W.; Zahan, N.; Hossain Firoz, F.; Azam, M. S. Bio-Inspired Immobilization of Silver and Gold on Magnetic Graphene Oxide for Rapid Catalysis and Recyclability. *J. Environ. Chem. Eng.* **2020**, *8*, 103739.
- (43) Wahab, M.; Zahoor, M.; Muhammad Salman, S.; Kamran, A. W.; Naz, S.; Burlakovs, J.; Kallistova, A.; Pimenov, N.; Zekker, I. Adsorption-Membrane Hybrid Approach for the Removal of Azithromycin from Water: An Attempt to Minimize Drug Resistance Problem. *Water* **2021**, *13*, 1969.
- (44) Kifayatullah, H.; Tahir, H.; Shah, A. Modeling and Optimization of Ultrasound-Assisted Adsorption of Crystal Violet Dye by Graphene Oxide Nanoparticles Using Response Surface Methodology. *International Journal of Environ. Anal. Chem.* **2020**, *7*, 1–17.
- (45) Huang, H.; Wang, Y.; Zhang, Y.; Niu, Z.; Li, X. Amino-Functionalized Graphene Oxide for Cr(VI), Cu(II), Pb(II) and Cd(II) Removal from Industrial Wastewater. *Open Chem.* **2020**, *18*, 97–107.
- (46) Yasmin, S.; Shamsuddin Ahmed, M.; Jeon, S. A Noble Silver Nanoflower on Nitrogen Doped Carbon Nanotube for Enhanced Oxygen Reduction Reaction. *Int. J. Hydrogen Energy* **2017**, *42*, 1075–1084.
- (47) Emiru, T. F.; Ayele, D. W. Controlled Synthesis, Characterization and Reduction of Graphene Oxide: A Convenient Method for Large Scale Production. *Egypt. J. Basic Appl. Sci.* **2017**, *4*, 74–79.
- (48) Yasmin, S.; Roy, N.; Kabir, M. H.; Jeon, S. Nitrogen-Functionalized Carbon Nanotube Based Palladium Nanoparticles as an Efficient Catalyst for Oxygen Reduction and Ethanol Oxidation Reaction. *Appl. Surf. Sci. Adv.* **2022**, *9*, 100235.
- (49) Al-Gaashani, R.; Najjar, A.; Zakaria, Y.; Mansour, S. XPS and Structural Studies of High Quality Graphene Oxide and Reduced Graphene Oxide Prepared by Different Chemical Oxidation Methods. *Ceram. Int.* **2019**, *45*, 14439.
- (50) Valencia, C.; Valencia, C.; Zuluaga, F.; Valencia, M.; Mina, J.; Grande-Tovar, C. Synthesis and Application of Scaffolds of Chitosan-Graphene Oxide by the Freeze-Drying Method for Tissue Regeneration. *Molecules* **2018**, *23*, 2651.
- (51) Ickecan, D.; Zan, R.; Nezir, S. Eco-Friendly Synthesis and Characterization of Reduced Graphene Oxide. *J. Phys.: Conf. Ser.* **2017**, *902*, 012027.
- (52) Faniyi, I. O.; Fasakin, O.; Olofinjana, B.; Adekunle, A. S.; Oluwasusi, T. V.; Eleruja, M. A.; Ajayi, E. O. B. The Comparative Analyses of Reduced Graphene Oxide (RGO) Prepared via Green, Mild and Chemical Approaches. *SN Appl. Sci.* **2019**, *1*, 1181.
- (53) Azam, Md. G.; Kabir, M. H.; Shaikh, Md. A. A.; Ahmed, S.; Mahmud, M.; Yasmin, S. A Rapid and Efficient Adsorptive Removal of Lead from Water Using Graphene Oxide Prepared from Waste Dry Cell Battery. *J. Water Proc. Eng.* **2022**, *46*, 102597.
- (54) Tan, P.; Bi, Q.; Hu, Y.; Fang, Z.; Chen, Y.; Cheng, J. Effect of the Degree of Oxidation and Defects of Graphene Oxide on Adsorption of Cu²⁺ from Aqueous Solution. *Appl. Surf. Sci.* **2017**, *423*, 1141–1151.
- (55) Guerrero-Fajardo, C. A.; Giraldo, L.; Moreno-Piraján, J. C. Preparation and Characterization of Graphene Oxide for Pb(II) and Zn(II) Ions Adsorption from Aqueous Solution: Experimental, Thermodynamic and Kinetic Study. *Nanomaterials* **2020**, *10*, 1022.
- (56) Noor, N. A. M.; Kamarudin, S. K.; Darus, M.; Yunus, N. F. M.; Idris, M. A. Photocatalytic Properties and Graphene Oxide Additional Effects in TiO₂. *Solid State Phenom.* **2018**, *280*, 65–70.
- (57) Kim, S.-G.; Park, O.-K.; Lee, J.; Ku, B. Layer-by-layer assembled graphene oxide films and barrier properties of thermally reduced graphene oxide membranes. *Carbon Lett.* **2013**, *14*, 247.
- (58) Aliyev, E. M.; Khan, M. M.; Nabiyev, A. M.; Alosmanov, R. M.; Bunyad-zadeh, I. A.; Shishatskiy, S.; Filiz, V. Covalently Modified Graphene Oxide and Polymer of Intrinsic Microporosity (PIM-1) in Mixed Matrix Thin-Film Composite Membranes. *Nanoscale Res. Lett.* **2018**, *13*, 359.
- (59) Singh, A. K.; Basavaraju, K. C.; Sharma, S.; Jang, S.; Park, C. P.; Kim, D.-P. Eco-Efficient Preparation of a N-Doped Graphene Equivalant and Its Application to Metal Free Selective Oxidation Reaction. *Green Chem.* **2014**, *16*, 3024–3030.
- (60) Lin, C.-Y.; Yang, D.-H. Removal of Pollutants from Wastewater by Coal Bottom Ash. *J. Environ. Sci. Health, Part A: Environ. Sci. Eng.* **2002**, *37*, 1509–1522.
- (61) Zhang, S.; Dong, Y.; Yang, Z.; Yang, W.; Wu, J.; Dong, C. Adsorption of Pharmaceuticals on Chitosan-Based Magnetic Composite Particles with Core-Brush Topology. *Chem. Eng. J.* **2016**, *304*, 325–334.
- (62) Saadi, Z.; Fazaali, R.; Vafajoo, L.; Naser, I.; Mohammadi, G. Promotion of Clinoptilolite Adsorption for Azithromycin Antibiotic by Tween 80 and Triton X-100 Surface Modifiers under Batch and Fixed-Bed Processes. *Chem. Eng. Commun.* **2020**, *208*, 328.
- (63) Martins, A. C.; Pezoti, O.; Cazetta, A. L.; Bedin, K. C.; Yamazaki, D. A. S.; Bandoch, G. F. G.; Asefa, T.; Visentainer, J. V.; Almeida, V. C. Removal of Tetracycline by NaOH-Activated Carbon Produced from Macadamia Nut Shells: Kinetic and Equilibrium Studies. *Chem. Eng. J.* **2015**, *260*, 291–299.
- (64) Zhang, D.; Yin, J.; Zhao, J.; Zhu, H.; Wang, C. Adsorption and Removal of Tetracycline from Water by Petroleum Coke-Derived Highly Porous Activated Carbon. *J. Environ. Chem. Eng.* **2015**, *3*, 1504–1512.
- (65) Samarghandi, M.; Al-Musawi, T.; Mohseni-Bandpi, A.; Zarrabi, M. Adsorption of Cephalexin from Aqueous Solution Using Natural Zeolite and Zeolite Coated with Manganese Oxide Nanoparticles. *J. Mol. Liq.* **2015**, *211*, 431–441.
- (66) Cortés Arriagada, D.; Sanhueza, L.; Wrighton, K. Removal of 4-Chlorophenol Using Graphene, Graphene Oxide, and a-Doped Graphene (A = N, B): A Computational Study. *Int. J. Quant. Chem.* **2013**, *113*, 1931–1939.
- (67) Swathi, R. S.; Sebastian, K. L. Long Range Resonance Energy Transfer from a Dye Molecule to Graphene Has (Distance)–4 Dependence. *J. Chem. Phys.* **2009**, *130*, 086101.
- (68) Gao, Y.; Li, Y.; Zhang, L.; Huang, H.; Hu, J.; Shah, S. M.; Su, X. Adsorption and Removal of Tetracycline Antibiotics from Aqueous Solution by Graphene Oxide. *J. Colloid Interface Sci.* **2012**, *368*, 540–546.
- (69) Zhu, D.; Pignatello, J. J. Characterization of Aromatic Compound Sorptive Interactions with Black Carbon (Charcoal) Assisted by Graphite as a Model. *Environ. Sci. Technol.* **2005**, *39*, 2033–2041.
- (70) Xu, J.; Wang, L.; Zhu, Y. Decontamination of Bisphenol A from Aqueous Solution by Graphene Adsorption. *Langmuir* **2012**, *28*, 8418–8425.
- (71) Sobhanardakani, S.; Zandipak, R.; Sahraei, R. Removal of Janus Green Dye from Aqueous Solutions Using Oxidized Multi-Walled Carbon Nanotubes. *Toxicol. Environ. Chem.* **2013**, *95*, 909–918.
- (72) Ciopec, M.; Davidescu, C. M.; Negrea, A.; Grozav, I.; Lupa, L.; Negrea, P.; Popa, A. Adsorption Studies of Cr(III) Ions from Aqueous Solutions by DEHPA Impregnated onto Amberlite XAD7 – Factorial Design Analysis. *Chem. Eng. Res. Des.* **2012**, *90*, 1660–1670.
- (73) Al-Ghouti, M. A.; Al-Absi, R. S. Mechanistic Understanding of the Adsorption and Thermodynamic Aspects of Cationic Methylene Blue Dye onto Cellulosic Olive Stones Biomass from Wastewater. *Sci. Rep.* **2020**, *10*, 15928.
- (74) Mehrdoost, A.; Jalilzadeh Yengejeh, R.; Mohammadi, M. K.; Babaei, A. A.; Haghghatzaheh, A. Comparative Analysis of UV-Assisted Removal of Azithromycin and Cefixime from Aqueous Solution Using PAC/Fe/Si/Zn Nanocomposite. *J. Health Sci. Surveill. Syst.* **2021**, *9*, 39–49.
- (75) de Sousa, D. N. R.; Insa, S.; Mozeto, A. A.; Petrovic, M.; Chaves, T. F.; Fadini, P. S. Equilibrium and Kinetic Studies of the Adsorption of Antibiotics from Aqueous Solutions onto Powdered Zeolites. *Chemosphere* **2018**, *205*, 137–146.
- (76) Sayadi, M. H.; Sobhani, S.; Shekari, H. Photocatalytic Degradation of Azithromycin Using GO@Fe₃O₄/ ZnO/ SnO₂ Nanocomposites. *J. Cleaner Prod.* **2019**, *232*, 127–136.